Journal of Thermal Analysis and Calorimetry
https://doi.org/10.1007/s10973-022-11374-9

DTA/TGA/DSC and densification data for iron phosphate glasses having natural $UO_{2.67}$ or surrogate Bi_2O_3 added

Paula A. Arboleda[1,2] · Jesús Ma. Rincón[3] · Carlos J. R. González Oliver[2,4]

Received: 10 October 2021 / Accepted: 16 April 2022

Abstract
A new set of iron-uranium phosphate glasses containing (1–20) $UO_{2.67}$. (10–20) Fe_2O_3. (55–68) P_2O_5 (mass/%) were melted adequately. They were tested for glassy matrices to immobilize hazardous wastes such as radioactive ones. Likewise, new compositions had uranium oxide replaced with Bi_2O_3. Differential Thermal Analysis (DTA), Thermogravimetric Analysis (TGA), Differential Scanning Calorimetry (DSC), and dilatometry measurements allowed us to study the thermal properties. TGA runs on phosphate glasses containing Fe and U oxides indicated that on heating the glasses, up to T_S (dilatometric softening point), the Fe^{2+} ions oxidized irreversibly to Fe^{3+} ions which can increase the thermal stability of the glasses by delaying (or even avoiding) crystallization. The densification behavior, applied to pressed powder pellets of ground glasses, from controlled heating rate (CHR) runs (Δl/lo versus T/K), shows relative sample length change versus temperature during heating, provided further thermal data like densification details as well as definition of ranges of creep stability. Various DTA, DSC methods allowed estimating the activation energy for crystallization of these kind of glasses. In addition, separate crystallization treatments for a particular composition provided samples suitable to study the shape and content of crystals with the Scanning Electron Microscope (SEM)/Energy-Dispersive X-ray Spectroscopy (EDS) technique. Thus, a new family of iron-phosphate glasses having Na_2O, Al_2O_3 added (RR6—RR62—RR63) is presented and discussed here and compared to various glasses (like PFeOx and PFeUOx) previously developed at the Bariloche Atomic Center, Argentina (CAB) for radioactive waste immobilization. Activation energies depicted roughly similar values for viscous flow densification of glasses melted with controlled amounts of UO_2 for the earlier compositions as well as for the new formulations.

Keywords Iron phosphate glasses · Thermal methods · Densification · Uranium oxide · Bismuth oxide · Nuclear wastes

Introduction

For several decades, vitrification has presented itself as a promising technology for conditioning, in preparation for the final disposal of radioactive wastes [1–3]. Among other applications: like metals sealing, photonics, medical and health care; vitrification of radioactive wastes is a promising solution in isolating these types of residues.

In this sense, years ago [4], iron phosphate glasses immobilized a wide range of wastes due to their stable thermal properties, with lower transformation temperatures and higher thermal expansion coefficients than silicates. In addition, they have good chemical durability and elevated radiation resistance. On the other hand, some drawbacks of phosphate glasses were low chemical durability and a tendency to crystallize. However, with the addition of iron oxide, these types of phosphate glasses are more durable.

Thus, since 2012, other research groups have paid attention to the obtention and characteristics of these types of glasses. Ciecinska and Stoch [5] synthesized glasses of $55P_2O_5$- (10–19) Al_2O_3- (10–15) Fe_2O_3- (15–24) Na_2O (mass/%) and investigated their mechanical activation. Those same authors [6] considered the composition: $60P_2O_5$- $20Fe_2O_3$- $20Al_2O_3$ (mass/%) for immobilizing

✉ Jesús Ma. Rincón
rinconjma@gmail.com

1 Dirección de Asuntos Nucleares, Servicio Geológico Colombiano, Cra 50 # 26 - 20, 111321 Bogotá, Colombia

2 Centro Atómico Bariloche (CAB), Av. E. Bustillo, 9500 – 8400 S. C. de Bariloche, RN, Argentina

3 Depto de Agroquímica y Medio Ambiente, UMH, Avda. Universidad, s/n, 03202 Elche, Alicante, Spain

4 C.O.N.I.C.E.T, Godoy Cruz 2290 (C1425FQB), CABA, Argentina

Published online: 31 May 2022

saline nuclear wastes and obtained the maximum durability for the Fe/P = 0.67 ratio. The tetrahedral FeO_4^- compensate charges in the AlO_4^- tetrahedra. More complex glasses in the P_2O_5-SiO_2-K_2O-MgO-CaO-Fe_2O_3 glasses [7, 8] were spectroscopically analyzed by Fourier Transform Infrared Spectroscopy (FTIR) to determine the molar volume and the crystallization induced by the Fe^{2+}/Fe^{3+} ratio. The crystallization stability decreases for higher Fe^{2+} contents. More recently, Goj et al. [9] studied Na_2O-30Fe2O3-70P2O5 (mol/ %) glasses. The P-O-P bridges hydrolyze strongly, while the P-O-Fe bridges showed themselves to be more resistant. All the characteristics of glassy state parameters given in [9], allowed a comparison with the formation of iron phosphate and sodium iron pyrophosphate crystalline phases.

Iron (III) oxide additions are conducive to the significant improvement of chemical durability, and additional properties are improved by adding various oxides of different valence to the original phosphate network. Some high-level nuclear waste (HLW), as is at Hanford, US-WA [10], contain phosphates up to 15 mass/% P_2O_5, iron oxides (up to 25 mass/%), and other heavy metal oxides, such as Bi_2O_3 up to 30 mass/% and uranium (up to 30 mass/% UO_2). Because of high P_2O_5 and heavy metals content, there is a concern [11] about phase separation or liquid immiscibility that P_2O_5 can produce in borosilicate glasses, such as those now used for vitrifying nuclear wastes. When a glass undergoes phase separation, its properties, such as chemical durability, usually changes [12].

For this work, the changes in the thermal behavior of a series of iron phosphate glasses, which incorporate about 20 mass/% $UO_{2.67}$ and Bi_2O_3, plus small additions of MgO, Al_2O_3 and Na_2O provoking changes in the glass characteristics can provide useful data to consolidate or sinter iron phosphate glassform, using the related fine glassy-grains. The enrichment in Al_2O_3 and MgO in turn can improve the chemical durability of the final wasteform. On the other hand, by using Bi_2O_3 as surrogate instead of $UO_{2.67}$ in some compositions can facilitate the investigation at laboratory scales for avoiding some radioactivity, though in any case all glasses here investigated include low levels of natural uranium.

Materials and methods

Table 1 shows the original theoretical composition, whereas Tables 2 and 3 do so for the final compositions after melting and pouring. They are a wide range of compositions designed in previous investigations lately reported, others newly melted and including Bi_2O_3 as surrogate as also new compositions. The melting process was carried out by heating the batches at 1473–1573 K in commercial alumina crucibles containing ~ 2 mass/% MgO in a Deltech DT-31 furnace ~ 2 h under static air, and they were cast in steel molds. The raw materials were previously mixed and treated in a ceramic porcelain vessel (Nanoker, Spain) at 1 K min^{-1} till 973 K for 1 h; specifically, these were $NH_4H_2PO_4$ (99.5% pure) CABAL Chemical Product (Brazil), Fe_2O_3 Berna (Argentina), Na_2CO_3 Cicarelli (Argentina), and U_3O_8 (Dioxitec, Argentina). Glass specimens of elongated prism bar shapes heated at 0.5 K min^{-1} to 763 K, maintained for 15 min at 763 K, and then cooled at furnace rate, showed good annealing properties at room temperature (RT). All the final specimens were amorphous as checked by X-ray diffraction (XRD) using a Phillips PW 1700 diffractometer with radiation of CuK_α-wavelength (0.154054 nm).

In relation to identification, from the DTA (Differential Thermal Analysis) curve of a given glass, procedures of DTA glass thermal parameters: T_g (Transformation temperature), T_C (crystallization temperature), ΔH_C (crystallization enthalpy), T_m (melting or liquidus temperature), ΔH_f (heat of fusion) and other parameters are mentioned in references [13, 14]. For dilatometer thermal expansion parameters T_g, T_S (glass softening temperature) and expansion coefficients the reader can refer to Zarcycki monographic book [15]. As is usual for glasses, simplified sketches indicating how to define the above parameters are shown in Fig. 1. It is shown a DTA curve for a simple silicate glass composition exhibiting high crystallization

Table 1 Initial batches (nominal compositions) of glasses recently investigated in the UO_2-Fe_2O_3-P_2O_5 system

Mass/% Code	P_2O_5	Fe_2O_3	UO_2	Bi_2O_3	Na_2O	MgO
RR6	58.80	19.60	19.60	–	2.00	–
RB6	58.80	19.60		19.60	2.00	–
RB7	69.32	18.53	–	10.15	2.00	–
RB6M	56.50	16.00	–	17.50	–	10.00
RR62	56.95	18.28	18.77	–	6.00	–
RR7	69.32	18.53	10.15	–	2.00	–
RR60	59.40	20.20	20.40	–	–	–
RR63	55.00	16.00	16.50	–	12.50	–

Table 2 Final compositions and thermal properties determined for earlier glasses [18, 19] and AR series glasses [18, 19, 24]

Mass/% Code	P_2O_5	MgO	Al_2O_3	SiO_2	Fe_2O_3	Na_2O	UO_2	T_g/K*	T_s /K **	CTE $\times 10^{-7}$/K^{-1}*
CAB1	63.42	–	2.43	–	34.15	–	–	756	777	36
CAB2	68.27	–	3.42	–	28.30	–	–	755	783	87
DR1	60.33	–	3.56	–	30.85	–	5.26	759	781	45
DR2	56.58	–	3.47	–	26.24	–	13.71	766	792	28
PFeOx	62.40	–	6.11	7.61	16.41	7.37	–	776	804	90
PFeUOx	60.00	–	6.18	5.70	14.77	6.41	6.94	799	832	85
AR1	53.70	1.90	2.10	–	27.00	2.30	12.90	769	812	26
AR4	45.80	1.60	1.90	–	42.20	2.30	6.20	777	804	89
AR5	46.2	1.80	1.70	–	35.40	2.30	12.50	776	805	108
AR6	57.30	2.10	1.70	–	18.40	2.30	18.20	812	862	34

*From dilatometric measurements carried out at 5 K min^{-1}

**(T_g glass transformation temperature, T_s dilatometric softening temperature, *CTE* coefficient of thermal expansion)

Table 3 Final compositions and thermal properties for recent RRx and RBx glasses

Mass/% Code	P_2O_5	MgO	Al_2O_3	Fe_2O_3	Na_2O	UO_2	Bi_2O_3	T_g (K)	T_s (K)	T_C (K) *	CTE $\times 10^{-7}$ (K^{-1})
RR6	59.37	2.10	2.18	15.52	2.00	18.83	–	794	895	898	106
RB6	59.00	2.80	3.20	15.00	3.40	–	16.60	784	810	~976	128
RB7	64.50	2.77	5.03	15.70	3.00	–	9.00	800	889	~973	31
RB6M	66.40	5.80	2.00	13.70	–	–	12.10	797	832	1021	57
RR62	59.26	3.3	5.28	12.38	6.67	13.11	–	833	857	–	77
RR7	65.20	–	3.40	13.12	4.22	14.06	–	~808	~863	1113	159
RR60	59.81	1.87	1.89	17.78	–	18.65	–	831	853	947	30
RR63	57.52	2.42	2.80	11.27	9.82	16.17	–	824	849	922	182

T_C crystallization temperature taken as the maximum of exothermic peak by the DTA method

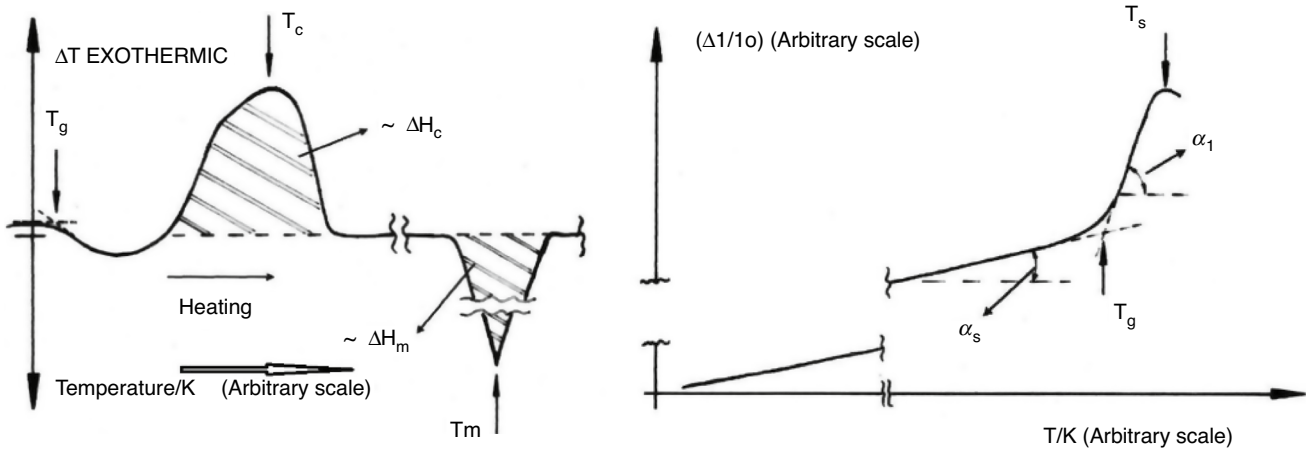

Fig. 1 Schematic representation of DTA curve (left drawing) for a powdered glass heated at constant heating rate from room temperature to the melting point. Thermal expansion curve (right sketch) of a solid glass bar re-heated at the same absolute rate to which the glass was cooled from T_s

tendency together with parameters Tg (marked by cross tangents to the endothermic deviation from de base line), T_C, T_m and the areas, proportional to respectively ΔH_C and ΔH_f, under de crystallization complex exothermic curve and melting endothermic peak. The thermal expansion curve in this Fig. 1 corresponds to a given glass subjected to a heating rate of absolute value similar to the cooling rate of the glass. Graphical definitions of thermal points and thermal expansion (α) coefficients are shown. They correspond to T_g, T_S, T_m and α_S ´solid like´ thermal expansion and α_l ´liquid like´ ($Tg < T < T_S$) thermal expansion of a typical well annealed glass. For the DTA curve the T_g, T_C and the areas under the crystallization- and melting-peaks are functions of the heating rate. T_g in both DTA and dilatometer curves is a function of the heating rate.

In order to simplify the reading of this paper, some of the thermal properties grouped and listed in Table 2, like T_g, CTE (or also α coefficient), and T_s, were the glass transition temperature T_g by differential thermal analysis (DTA)/differential scanning calorimetry (DSC), the coefficient of thermal expansion (CTE), and dilatometric softening point T_s by dilatometry analysis. Specimens 1.5 mm thick, cut from annealed bulk glass, allowed the measurement of linear thermal expansion of the glasses. Differential vertical dilatometer Theta Dilatronics II equipment was used at heating rates of 2–5 K min^{-1} under constant O_2 flow. The data were corrected with a piece of calibrated bulk of silica glass and quoted as $\Delta l/lo = [l_{(T)} - l_o]/l_o$; where $l_{(T)}$ and l_o represent, respectively, the instantaneous length and the initial length of the sample**.** The errors for Δl/lo are less than 3% and for T measurement ± 3 K, respectively. Crushed, ground and sieved powders with particle size below 75 µm were used for DTA measurements carried out in a Universal VIIIATA at 10 $Kmin^{-1}$ at constant O_2 flow. TGA was made in TA SDQ Q600 equipment. The DSC runs were carried out at various heating rates in a SETARAM apparatus using powder samples sifted at 75 µm.

The final compositions of polished samples (Table 3) were determined with X-ray energy-dispersive spectroscopy (EDS), using an Edax® detector attached to a Philips 515 scanning electron microscope (SEM) and mapping element over the sample surface with a FEI NovaNano 230 SEM/field emission gun (FEG).

The compositions of the glasses in Table 3, designed with increasing Na_2O content for enhancing the glassy matrix fluidity, where the radioactive waste remains in a more homogeneous distribution without losing much of the chemical durability resistance, contain important quantities of UO_2 (or Bi_2O_3), as is usual in high simulated waste. The substitution of U by Bi has allowed us to investigate these simulated nuclear wastes without using dangerous radionuclides in the laboratory.

Results

Glass melting and final compositions

With respect to the melting process, the schedule conditions: homogenization of batch, crucible, time of melting, oven, and others are very sensitive to the resulting final compositions of these types of phosphate glasses. In general, the nominal calculated values are quite different with respect to the final measured compositions (Tables 1 and 3). Because this research extended for several years, it is necessary to indicate that the ARx series of glasses obtained eight years before the RRx series was not the same (Table 2). Furthermore, these melted glasses usually show very strong composition variations due to the volatilization of several oxides during melting and uncontrolled alumina (doped with MgO) crucible corrosion. The presence of Al_2O_3 and MgO to a significant extent is a consequence of crucible corrosion during the melting process [12]. These oxides can cause notable modifications to the thermal properties, like glass transition temperature T_g, dilatometric softening point T_s, and the linear CTE (α in other publications). In addition, they can alter the crystallization trend of the glass and its chemical durability properties. MgO intentionally added in the design of RB6M (RBx series), can change the thermal performance of the modified glass. Therefore, it is important to infer the modification effect of this oxide on the vitreous network. Thus, Tables 1, 2, and 3, respectively, include the compositions for the previous glasses investigated, the theoretical compositions of new glasses, and the compositions of final glasses, which are the main object of the following discussions.

Similarly, Na_2O was added for some compositions, such as RR6, RR62, and RR63, aiming to lower the waste glass viscosity. That is, the radioactive waste or spent fuel with mainly uranium oxide could show better dispersion/homogenization properties within the matrix of iron-phosphate glass after melting to obtain the wasteform or after the densification of the corresponding pressed pellet (made of powdered glass). In previous works [17–19], the viscosity of the corresponding iron-phosphate glasses increased strongly for the UO_2 additions. Therefore, additions of Na_2O, plus small adjustments with alumina, could be justified to improve the residue distribution within the glassy matrix.

Thermal behavior of new glasses

The thermal expansion coefficient (CTE, or α), the glass transformation point (T_g), the softening point (T_s), and

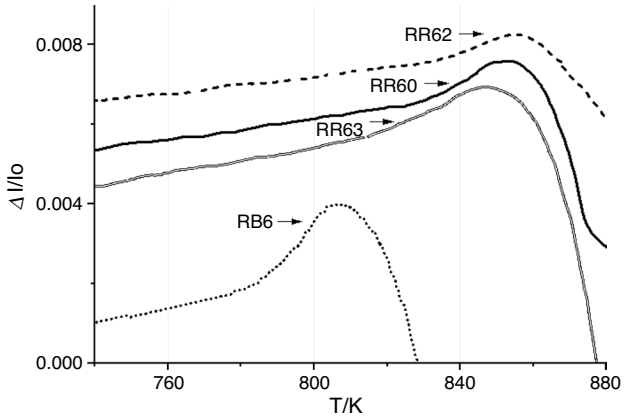

Fig. 2 Dilatometric result of final solid glasses from the RR6 series and that of the RB6 composition

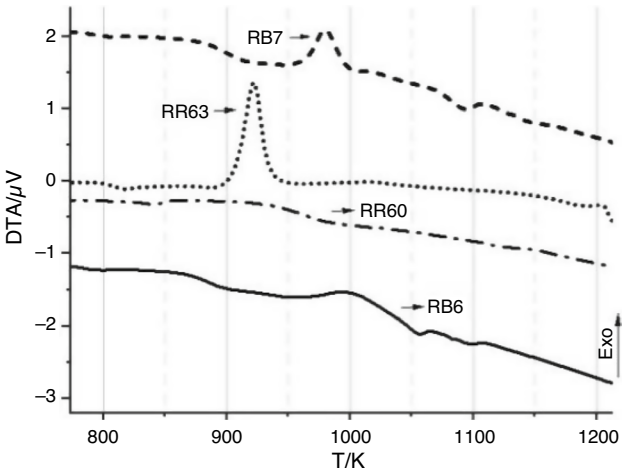

Fig. 3 DTA curves for the RR and RB iron phosphate new glasses

liquidus temperature (T_l) were calculated according to dilatometry data (Fig. 1). Tables 2 and 3 list the obtained values; the CTE was calculated from the slope of lines, interpolating the $\Delta l/l_o$ data and T_g by the intersection of the two lines (for the low and high-temperature ranges (Fig. 1). These curves in the glass transformation range suggest the glasses behave as expected concerning T_g reversibility. The apparent T_g shifts to higher temperatures by increasing the heating rate and, conversely, lowering the heating rate (Fig. 2). The reference [18] fully shows the thermal expansion curves corresponding to the AR series of glasses. From Table 3 and Fig. 2, by increasing the Na_2O content (9.82% Na_2O) and decreasing the Al_2O_3 level (2.8% Al_2O_3) for RR63 (having 16.2 mass/% UO_2) as compared to RR62 (13.1 mass/% UO_2), the softening point T_S and Tg decreased markedly for RR63 with respect to glass RR62. Also, the thermal expansion of RR63 increased significantly relative to that of RR62. The lower thermal expansion for RR62, the reasonable levels of 6.7% Na_2O and 5.3% Al_2O_3 extra oxide additions, the higher T_S of 857 K (584 °C), and the low tendency to crystallization (as indicated by a faint DTA-exothermal event) suggest this overall composition ´encapsulating´ 13.1% UO_2 as very promising to produce wasteform. However, there remains to measure the chemical durability of such a series of glasses.

Differential thermal analysis (DTA) and differential scanning calorimetry (DSC)

Figure 3 shows the DTA traces for the new RR and RB glasses. The corresponding glass transition temperature corresponded to the first endothermic peak of each glass sample. In some waste glasses, the traces showed clear exothermic peaks for compositions RR63 and RB7 related to crystallization phenomena. This exothermic behavior is related to the crystallization peaks of probably the following crystalline phases: $FePO_4$, $Fe^{3+}{}_2\,Fe^{2+}(P_2O_7)_2$, Fe $(PO_3)_3$, common phases also identified in previous research by Kuczek et al. [8]. Also, $FeUO_4$ was identified in the case of a novel glass RR63, including uranium; $FeUO_4$: iron (III) uranium (V) oxide, ICSD#24,963 [JCPDS732386], orthorhombic, unit cell 0.4888, 1.1937, and 0.5110 nm (see reference [18]).

The main crystalline iron phosphate phases found after simple heat treatments at specific exothermic temperatures were:

(i) $FePO_4$, JCPDS840876, iron phosphate (V), ICSD #201795, rodolicoite, trigonal/rhombohedral, unit cell 0.5027(2), 0.5027(2), and 1.1234(4) nm, respectively angles: 90, 90 and 120.
(ii) $Fe^{3+}{}_2\,Fe^{2+}\,(P_2O_7)_2$, JCPDS802315, iron diphosphate, ICSD #71129, orthorhombic, unit cell 0.89500(7), 1.2235(2), and 1.0174(1) nm; respectively angles: 90, 90 and 90.
(iii) Fe $(PO_3)_3$, JCPDS440772, iron (III) tris (phosphate (V)), ICSD #88848.

As noted in Table 3, for RB glasses, by increasing the Bi_2O_3 level (RB6), the Tg decreases relative to that for RB7, suggesting a weakening effect of the glass structure upon increasing the bismuth oxide content. This is the opposite effect as compared to the addition of UO_2 to similar iron phosphate glasses. By comparing RB6 and RB6M, the addition of MgO provokes Tg, T_S, and T_C values to increase. Thus, the increase in T_C (crystallization temperature) for glass RB6M makes it more stable toward devitrification.

Figure 4 shows the DSC results for the RR7 glass at different heating rates from 10 to 60 K min^{-1} where increasing crystallization exo-peaks (T_C written as T_P in the graph at right) from 1123 to 1188 K can be seen when this heating

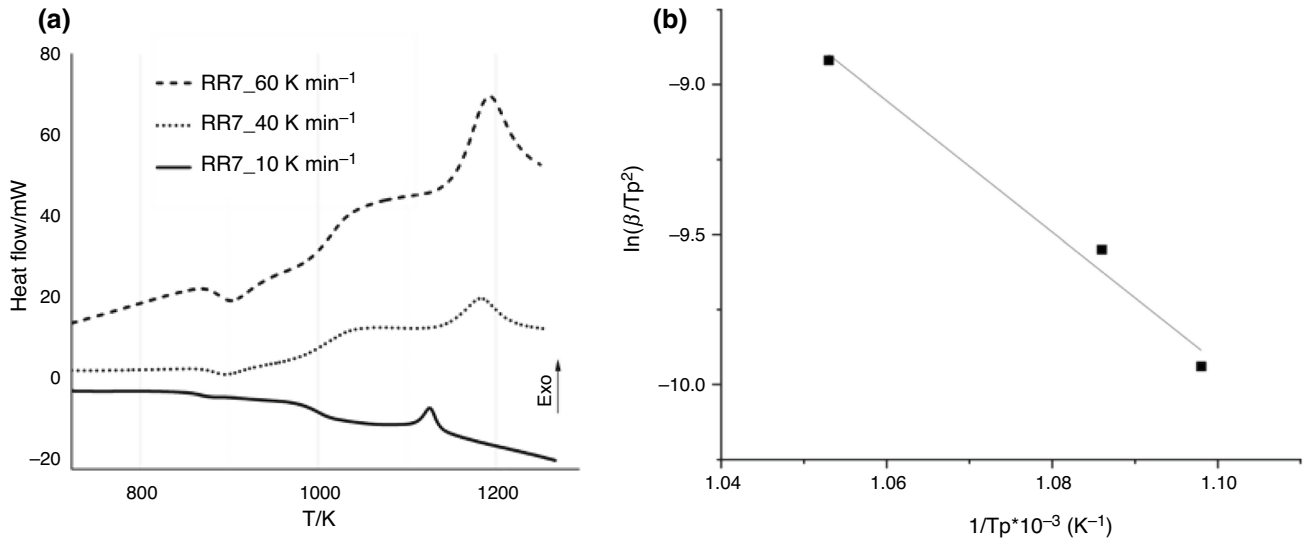

Fig. 4 **a** DSC graphs for RR7 powder samples at several heating rates: 10, 40, and 60 K min^{-1}; **b** Graph for the calculation of activation energy by following the Kissinger method

rate is augmented. To evaluate the activation energy for the crystallization exothermic peak, the well-known Kissinger model method was used [20, 21] by representing the ln (β/$T_p^{\,2}$) versus the $1/T_p * 10^{-3}$ (K^{-1}), where T_p is the exo-peak temperature and β the heating rate. This representation gave activation energy for crystallization of 184 ± 3 kJ mol^{-1}. From chemical composition and X-ray diffraction data for RR7 and AR7, given in [18], it could be assumed that the main crystallizing phase in RR7 can be Fe $(PO_3)_3$. While RR7 has more UO_2 and less Fe_2O_3 than AR7 (65% P_2O_5, 19% Fe_2O_3, 2.1% Na_2O, 2.6% Al_2O_3, 2.1% MgO, 9.1% UO_2 (mass/%), the main crystallization exo-peak occurs at ~ 1123 K, which is not far from the peak for AR7 at about 1078 K as can be seen later in Fig. 7. Therefore, this peak position difference can be due to the chemical compositions of both glasses. For AR7 heated up to 1048 K (O_2 flow, 1 h), the main crystalline phase was Fe $(PO_3)_3$ together with a small quantity of $UFeO_4$ (Fig. 5). Therefore, the main crystal phases for RR7 could also be Fe $(PO_3)_3$ and $UFeO_4$. As the heating rates in the DSC data in Fig. 4 (a) are quite high, the exotherms can be assigned to the main Fe $(PO_3)_3$ crystalline phase.

With respect to crystallization morphologies, several SEM, EDS microanalyses, carried out on polished RR7cr samples (crystallized glass RR7), at the exothermic peak from DSC, provided an estimation of the Fe/P and/or Fe_2O_3/UO_2 ratios to discriminate what types of the former crystalline phases are responsible for this activation energy. The RR7cr crystallized sample underwent the following treatment: 7 h until reaching its nucleation temperature (T_N: 898 K for 4 h) and then at a slow heating rate (1 K min^{-1}) until 1048 K for 6 min. As noted above, these crystals can

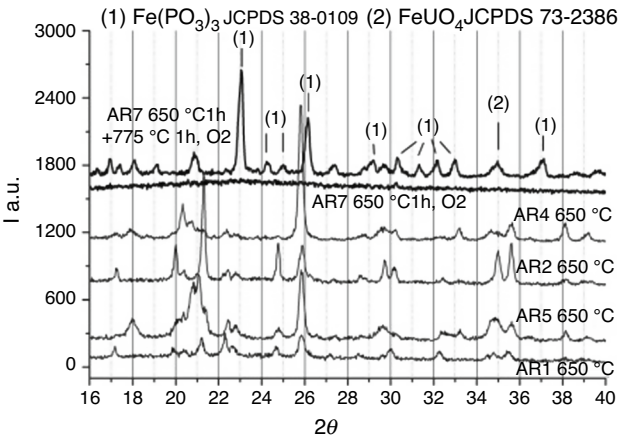

Fig. 5 XRD data for AR7 crystallized after heating up to (from 923 K) 1048 K for 1 h under oxygen flow. Also are shown X-ray difractograms for glasses AR1, AR2, AR4 and AR5 after heating up to 923 K, 1 h, O_2 flow

be Fe $(PO_3)_3$. The crystallized areas with spike-shapes and incipient dendritic growth begin on the surface like shown in the backscattered electron micrograph of Fig. 6 (a); similarly, a zoom zone covered noticeable interfaces (A, B, and C in Fig. 6 (b)). In addition, it gave an uniform chemical composition (Table 4) for the crystals and a different composition for the glassy phase showing strong component-gradients between the crystals and the mother glass.

It is relevant to consider an alternative method for calculating crystallization—activation energies proposed by Marotta et al. and reported in reviews [20, 21]. It relates to establishing the activation energy with only one DTA

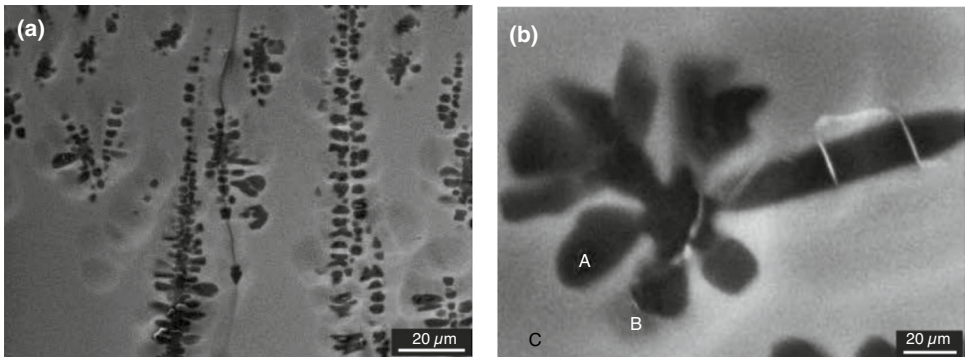

Fig. 6 **a** SEM micrographs of RR7cr (crystallized RR7 glass; see the text); the white bar denotes 20 μm; **b** The points A, B, and C correspond to spot EDS microanalysis in Table 4; the white bar denotes 2 μm

Table 4 EDS spot microanalysis in several areas of Fig. 6 (b) micrograph for the RR7 crystallized glass

Mass/%	P_2O_5	Fe_2O_3	UO_2	Na_2O	MgO
A Dark contrast dendrite	58.76	22.02	8.24	1.68	0.94
B Grey area near dendrite	57.08	24.37	7.45	1.77	0.58
C Residual white glassy area	63.24	15.23	11.07	1.43	2.13

Table 5 Activation energies for crystallization (heating rates 5–10 K min $^{-1}$) in the case of Marotta et al. method [21, 22]

Glass	T_{f1}/K	T_{f2}/K	ΔT	Volum]e E_{act}/kJ mol^{-1}	Surface E_{act}/kJ mol^{-1}
RR63	914	928	13	347	862
RR60	880	961	81	54	134
RB6	976	1029	53	100	251
RB7	973	988	15	331	845

diagram at 5 K min $^{-1}$. This approximated method uses the inflection temperatures of exothermic peaks T_{f1} and T_{f2} listed in Table 5, in Derivative Differential Thermal Analysis (DDTA) data from Fig. 3 and using the formula: $E/R(1/T_{f1} - 1/T_{f2}) = k$, with the value $R = 8.3145$ J mol^{-1} K^{-1}, with the constant $k = 1.59$ for surface crystallization and $k = 0.64$ for bulk crystallization. Thus, Table 5 lists the activation energies for crystallization evaluated by the Marotta et al. method for the iron phosphate glasses here investigated [22].

For both pairs, RR63/RR60 and RB7/RB6, 347/54, and 331/100 kJ mol^{-1} were obtained, respectively, for activation energies for bulk crystallization. For RB7 and RR63, the higher activation energy corresponds to the well-defined exothermic peak. Conversely, the less defined peak gives lower activation energy in RR60 and RB6 glasses.

In Fig. 7 are shown the DTA traces for the previously made glasses ARx (x: 1, 2, 4, 5, 6, 7) at 10 K min^{-1} under

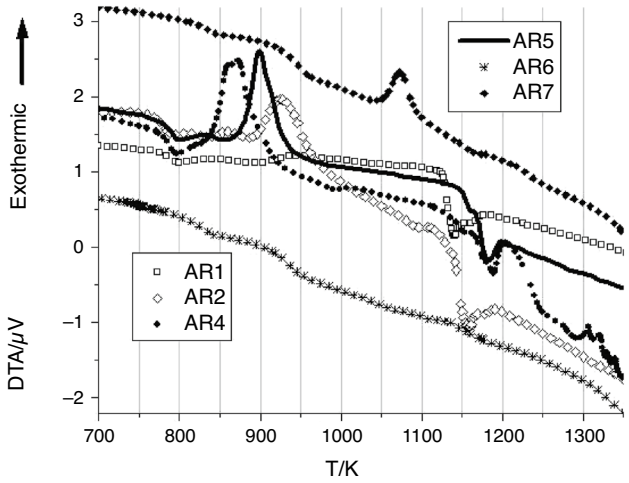

Fig. 7 DTA traces for glasses ARx

static air surrounding atmosphere and several remarks can be made [18]. For all glasses, the Tg is clearly detected. For AR2, AR4 and AR5 the crystallization peak T_C is seen clearly and for AR1, AR2, AR4 and AR5 the melting peak T_m (melting point or liquidus temperature) is apparently well-defined. Of relevance to this work, particularly for next "Thermogravimetric analysis (TGA)" section, is the fact that for pair AR4 (6.2% UO_2), AR5 (12.5% UO_2) the crystallization peak shifts to higher temperature, suggesting a kind of delay in crystallization by increasing the uranium oxide content of the glass. For this pair of glasses the main crystalline phases precipitated correspond to $Fe(PO_4)$ and Fe_2^{3+} Fe^{2+} $(P_2O_7)_2$, as was shown before in [18] and the crystal phases listed at the beginning of "Differential thermal analysis (DTA) and differential scanning calorimetry (DSC)" section.

Thermogravimetric analysis (TGA)

As noted above, it seems the crystallization-tendency of these iron phosphate glasses, with or without additions of

UO_2- waste, depends strongly on the oxidation states of iron. In previous works [23, 24], two Fe phosphate glasses were melted and examined for crystallization and chemical durability behaviors, they were named M4 and M5 and had chemical compositions M4: 61% P_2O_5; 26% Fe_2O_3; 7,5% SiO_2; 5,5% Al_2O_3 and M5: 67% P_2O_5; 13,2% Fe_2O_3; 10,9% UO_2; 5,3% SiO_2; 3,5% Al_2O_3. Experiments suggested: (i) XRD data at RT confirmed that M5, heated up to 1073 K, showed negligible crystallization. (ii) Upon heating in the air up to temperatures close to Tg, about 780 K for M4 and 850 K for M5, the powdered glasses gained mass as shown by the TGA traces; such increase in mass was assigned to the oxidation of Fe^{2+} ions into Fe^{3+} [23, 24]. (iii) On cooling, glass M5 did not change mass, whereas M4 clearly lost mass in an approximate opposite way than the heating cycle. Indirectly this might suggest that for UO_2 containing glasses, the iron is present mainly as Fe^{3+}.

Hereafter are presented new TGA runs, and Mössbauer spectra measurements are applied to the set of glasses: AR1, AR4, AR5, and AR6 (see Table 2). It was used a Shimadzu Simultaneous (TGA, DTA) Analyzer DTG-60Hn for the estimation of mass changes in airflow (50 mL min^{-1}) at temperatures close to their T_g -T_s ranges: 840 K (for AR1, AR5, and AR4) and 891 K (for AR6) during an elapsed time of 1 h. The T_g and T_S can be seen in Table 2 and ref. [18]. In these temperature ranges the glasses remained uncrystallized (Fig. 7).

Figure 8 shows the continuous TGA curves for the as-made glasses. It is noted that AR1, AR4, and AR5 glasses show an increase in mass during the 1 h isothermal treatment, at around 840 K, and little or no change for AR6 at 891 K. This effect may be assigned to different contents of Fe^{2+} and Fe^{3+} ions in the UO_2-waste containing glasses.

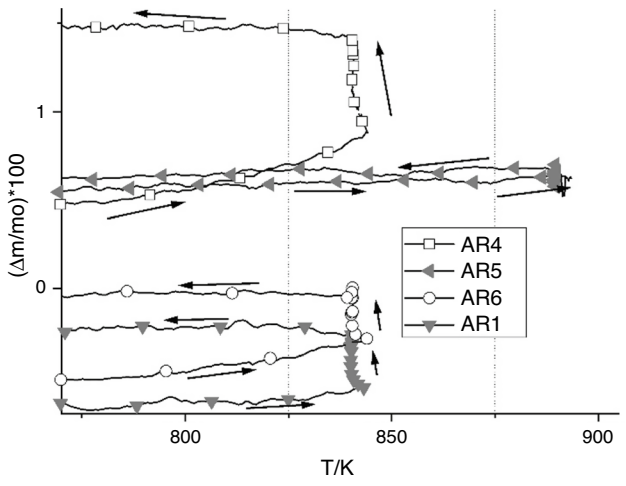

Fig. 8 TGA cycling, 1 h at 840 K or 891 K, after heating at a constant rate, of as-melted AR1, AR4, AR5, and AR6 under airflow of 50 mL min^{-1} (the symbols are only to guide the eyes for each glass)

It is relevant to note the increase in mass % for AR1, AR4 and AR5, after isothermal treatment, remained in that state down to room temperature (RT), after the whole TGA run. In Fig. 8, data are shown down to only 775 K but as stated before mass % was recorded down to RT and no loss in mass upon cooling was measured, for AR1, AR4 or AR5, that could indicate the conversion of Fe^{3+} into Fe^{2+}, as it was detected for sample M4 (having no addition of UO_2) described at the first paragraph of this section. The absolute (and corrected by the behavior of the empty crucible) relative mass/% changes [$(\Delta m/m_o)$ %; m_o: initial mass of glass] of the four glasses are quoted: AR1 = 0.27%, AR4 = 0.54%, AR5 = 0.22%, and AR6 = 0.00%. The main difference between AR4 and AR5 is related to the UO_2 content for AR5 (12.5% UO_2), which is double as compared to AR4 (6.2% UO_2), and this could explain the nearly double mass ($\Delta m/m_o$) % increase at 840 K for AR4. This can be interpreted as AR4 having a higher content of Fe^{2+} than AR5, provoking a higher overall crystallization for AR4 (and at lower temperatures as compared to AR5) of crystalline phases like $FePO_4$ for AR4 (Fig. 7). The AR5 glass, likewise contains a small amount of Fe^{2+} $Fe_2^{3+}(P_2O_7)_2$ crystal phase [18, 19].

The ratio-values ($Fe^{2+}/(Fe^{2+}+Fe^{3+})$), computed from the Mössbauer curves and PIXE/RBS [25] and deduced from the following Fig. 9 for AR1, AR4, AR5, and AR6 were: 0.2, 0.35, 0.22, and 0.04, respectively. That is, the higher ratio-values measured for AR4 (0.35) as compared to that for AR5 (0.22) correlates well with the greater overall crystallization obtained for AR4 and AR5 (Fig. 7).

Crystallization kinetic considerations should also be made as the viscosity of AR5 can be higher than that of AR4, reducing the molecular diffusion in AR5 and consequently explaining the lower tendency toward crystallization for AR5. Indeed, the T_S value was slightly lower for AR4

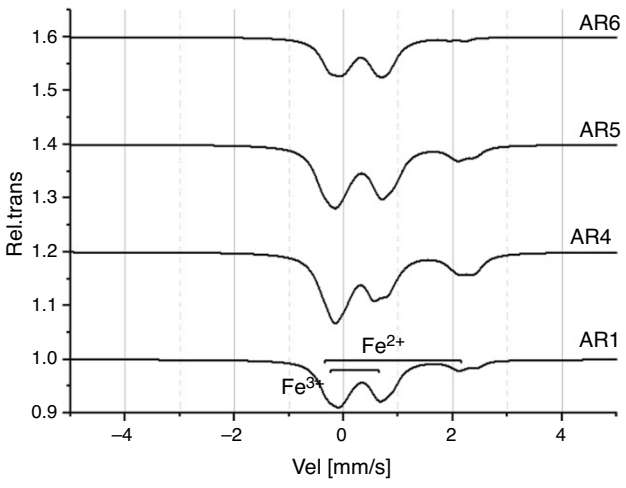

Fig. 9 Mössbauer spectra from the AR series glasses: AR1, AR4, AR5, and AR6

than AR5 suggesting a higher glass-viscosity for AR5. Also, the expansion coefficient in the ´liquid-like´ range between Tg and T_S [18] is lower for AR5 than for AR4, meaning a ´kind of stronger network´ for AR5 than for AR4. Furthermore, measuring the glass-viscosity and developing methods to determine the valence states of uranium (U^{4+}, U^{5+}, and U^{6+}) in these glasses could help check these arguments.

The closeness between the ($\Delta m/m_o$) % mass loss values are more difficult to explain for AR1 and AR5, by the previous proposal as the Fe-oxide content in AR5 is 8% higher while the UO_2 content is like that in AR1. This could happen if there are important changes in the valences of U ions during the experimental thermal treatment of 1 h in the air at 840 K.

The lack of ($\Delta m/m_o$) activity for AR6 glass appears to be related to the low Fe_2O_3 content and very high UO_2 level in this composition, such as during the melting, the U ions could fully oxidize the Fe ions. Thus, the conditions during pre-casting heat treatment are such that they fix the proper Fe^{2+}/Fe^{3+} ratio, still achieve satisfying melt and accurate wasteform properties. However, it is difficult to estimate precisely how these ($Fe^{2+}/(Fe^{2+}+Fe^{3+})$) fractions change with the composition, since it is depending on several other factors at the same time, such as: O/P and Fe/P, molar ratios, and the oxidation or reduction capacity of the other oxides that make up the glass [26].

Sintering of pressed pellets from powdered glasses

The field of making up waste forms by sintering or axial hot-pressing or HIP (hot isostatic pressing) pellets of glassy grains is a very active one. Moreover, it offers other possibilities, such as raising the stability of solid preforms and distributing the nuclear waste within the glassy matrix at lower temperatures than those involved in melting. This is useful to avoid important losses of the glass component, like, for instance, P_2O_5 and other oxides depicting a tendency to volatilize, such as Na_2O and UO_2. Therefore, we discuss the results after sintering similar compositions (to the molten ones) in the UO_2-Fe_2O_3-P_2O_5 system.

PFeOx and PFeUOx original glasses

Figure 10a shows the thermal expansion curves of solid (bulk) glasses for both PFeOx and PFeUOx glasses (see Table 2), and the linear densification ($\Delta l(T)/lo$ versus T (K)) established by dilatometer, run under O_2 flow at about 5.5 K min^{-1} heating rate of a pellet of powdered samples all made in the same manner for comparison purposes. In the dilatometer, the relative expansion or shrinkage is given by $\Delta l(T)/lo = \pm(lo - l(T))/lo$, where lo, l(T) are the initial and simultaneous heights of the specimen. Thus, the thermal expansion of PFeOx is greater than that for PFeUOx (Fig. 10a; Table 2), and both: T_g and T_S are lower for PFeOx than for PFeUOx, confirming a higher viscosity and a stronger network structure for the U-containing waste glass [17, 27]. Thus, it is clear that PFeUOx glass starts densifying at higher temperatures than PFeOx glass correlating well such temperature with T_S of the glasses. In addition, the overall densification rate is lower for PFeUOx than for PFeOx; this will be confirmed next from viscous flow activation energy calculations from these densification data. It should also be noted that both glasses appear to exhibit another densification mechanism after ending these initial stages of viscous flow mechanism at levels of about 15% absolute linear densifications; this could be related to the bulk Mackenzie-Shuttleworth mechanism [28].

As previously indicated, the sintering models for glasses and amorphous materials establish a mechanism of viscous flow, where the dependence of viscosity with temperature follows an Arrhenius type equation [27]. Therefore, the Frenkel densification rate for the initial viscous flow sintering [29] associated with only glassy particles may be described (Eq. (1)) as follows:

$$d[\Delta l(T)/lo]/dT = s[g/2acA]\exp(-E_a/RT) \quad (1)$$

where g and a are the surface tension and radius of the assumed spherical particles; c the heating rate; s a shape factor of value $s \sim 1$ for spherical grains and angular crushed particles $s \sim 5$. The viscosity of the glass is included in this equation as A exp (E_a/RT), where A contains entropy terms and E_a is the activation enthalpy for viscous flow. Assuming $s[g/2acA]$ does not change much with temperature, for a system obeying Eq. (1) a linear relationship between ln(d[$\Delta l(T)$/lo]/dT) and the variable (1/T (K)) should be obtained.

This estimation, performed for both pellet-glasses, gave the results shown in Fig. 10b–d compares both behaviors. For both glass compositions, it is roughly obtained that the linear Frenkel-plot within the initial 2–15% linear densification (see Eq. (1)) is well verified, and from the slope viscous flow-activation energies E_a of 132 and 189 kJ mol^{-1} for PFeOx and PFeUOx are obtained, respectively. This estimation confirms a higher viscosity glass for PFeUOx as compared to PFeOx.

Also, higher chemical durability was obtained for the $UO_{2.67}$ containing glass. It was argued that the U ions $U^{4+\text{ to }6+}$ may be positioned in between the phosphate chains (as modifiers) but somehow strengthen the glass structure to the high ionic field strength of U ions [27]. Therefore, such present matrices could be useful to encapsulate UO_2 residues and to make chemically stable iron phosphate glasses after the following two methods: (I) direct melting of the P-O-Fe–O-(Al, Si, Na)-U–O mass and casting bulky massive glassy forms; and, (II) by direct melting and quenching frit powders and subsequently

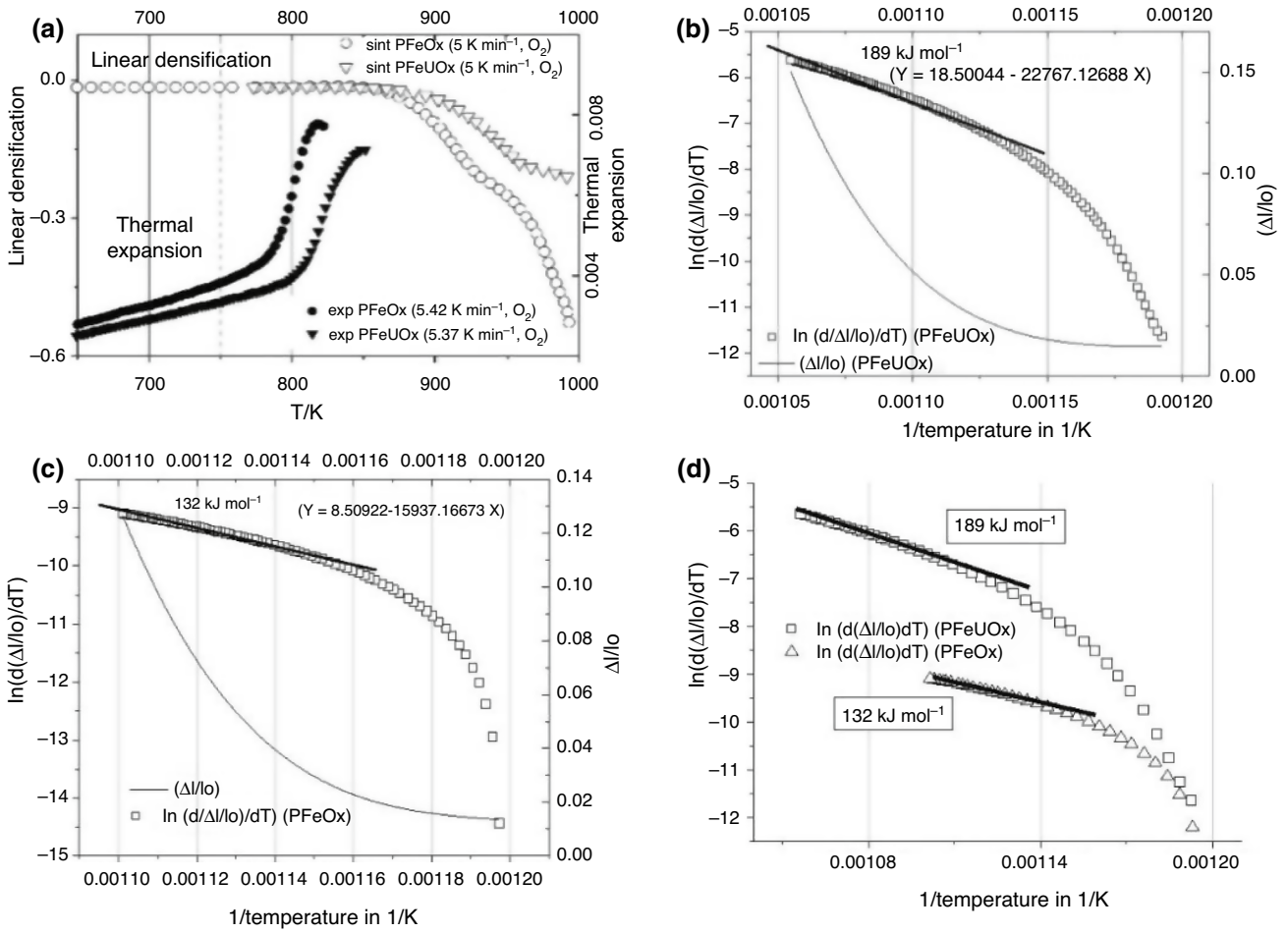

Fig. 10 Thermal sintering behavior of pressed pellets from original powdered glasses PFeOx and PFeUOx

sintering the porous pellet by direct heating as shown here in Fig. 10a or subjecting the pellet to hot pressing or hot isostatic pressing (HIP) schedules. Studying the crystallization properties or the tendency toward glass-in-glass phase separation in these compositions is relevant to the thermal stability evaluation. Also, it is expected that the Fe^{2+}–Fe^{3+} redox balance can be well controlled by the redox U^{4+}– U^{5+}– U^{6+} reaction; it is known that these iron phosphate glasses do crystallize more for higher Fe^{2+} content and that the presence of uranium ion balance can increase the oxidation state of the glass, making it more stable toward devitrification or crystallization [23, 24, 26].

The sintering of the RR6x (x = 0, 2, 3) new glass series

For the RR60, RR62, and RR63 series glasses with important UO_2 quantities and variable additions of Na_2O and Al_2O_3 to model the viscous flow properties of the final glasses, the sintering curves shown in Fig. 11a are measured with the dilatometer. However, there is not enough space available here for a complete discussion of the sintering behavior of the RR60, RR62, and RR63 powdered glass pellets, some kinetics findings equivalent to the previous analysis for powdered glasses PFeOx/PFeUOx are mentioned next. By fitting the Frenkel densification rate Eq. (1) above to RR60 and RR63 (see Fig. 11b), there were estimated activation energies; it was 586 kJ mol^{-1} for RR60.

Glassy powder RR63 has 9.8 mass/% Na_2O and shows extensive densification, giving activation energies E_a of 43 and 278 kJ mol^{-1} for two consecutive modes of densification (see Fig. 11b); this may have something to do with the size distribution of the glassy particles. The Frenkel model refers to the initial stage of densification by viscous flow. The Mackenzie-Shuttleworth intermediate/final stage sintering regime generally applies after the Frenkel stage [28, 29].

Figure 11a shows that the thermal shrinkage and expansion (Fig. 1, Table 3) behaviors of the RR6x (x = 0, 2, 3) series of glasses are quite similar. This would be somehow valid as the expansivities do not depend on the porosity of the sintered bodies. Nevertheless, there are differences in the

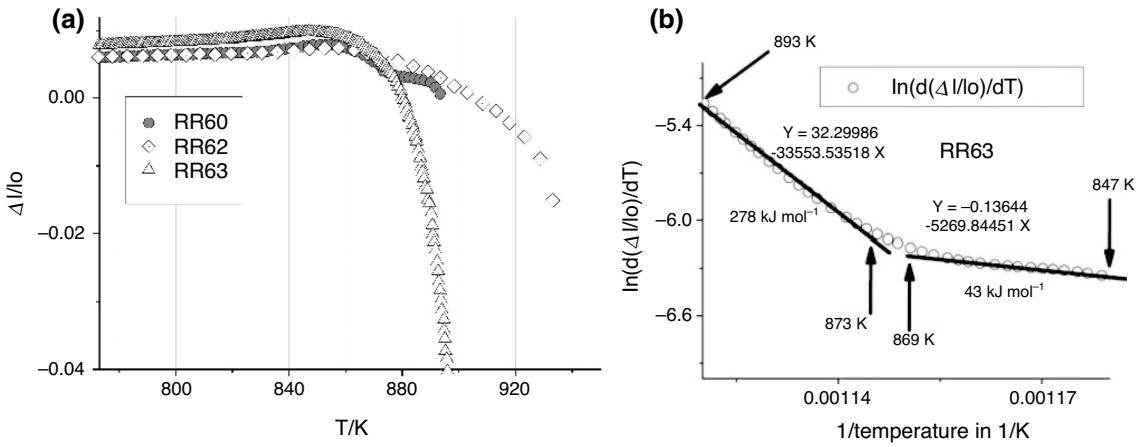

Fig. 11 **a** Dilatometric sintering curves for RR60, RR62, and RR63; **b** Frenkel plot for RR63 method given in [29]

temperature for the Tg transformation and for T_S softening points. Both glasses, RR62 and RR60, show a linear behavior in the thermal expansion until the T_S point. However, RR63 depicts T_S very clearly, and the Tg point is at 833 K, with T_S higher for RR62 than for RR60.

Other remarks concerning this Results Section include that by observing the possible exo-peaks responsible for crystallization [16], glasses with U and without uranium and with bismuth show wide exo-bands in the 923–1173 K interval. Thus, it seems that bismuth glass shows exo-peaks at 973–1003 K. In the case of RB6 glasses, the exo-peak is wider than in RB7 and RR7, indicating a tendency to low crystallization, that is, without very clear development of crystallization exotherms at the heating rates used in DTA experiments. Because this paper focused on the thermal behavior of new iron phosphate glasses investigated for immobilizing uranium wastes, it is worth mentioning that some chemical durability tests were carried out, and they are not reported here because they can be seen in references [17–19].

Discussion

The new glasses listed in Table 1 apply to compositions remelted recently, like RR6 and RR7, although they were melted almost a decade earlier, like AR1, AR5, AR6, and AR7, as fully described in references [17–19, 25, 27]. The final compositions differed significantly, probably owing to partial volatilizations and possible changes in final temperature and melting time. Also, the precursor for P_2O_5, ammonium phosphate (already mixed with the other batch components) must be fully decomposed at around 973 K. Then, this whole stage must be slowly made to avoid unwanted losses or reactions. It is noted that these basic 60 mol % P_2O_5. 40% Fe_2O_3 iron phosphate glasses, like [23, 27] old CAB1 and CAB2 from Table 2, can vitrify large amounts of UO_2 (equivalent to natural U_3O_8), being the main reason for selecting these base iron phosphate glasses to immobilize wastes with UO_2 content, at least, on a laboratory scale. Compositions like DR1/DR2, PFeOx/PFeUOx, and AR1/AR5, among others (see Table 2), were examined to dissolve the UO_2 residue successfully. During these melting in alumina crucibles containing MgO, considerable 1–3% enrichment in Al_2O_3 and MgO of the final glass composition was met owing to crucible-corrosion by the iron phosphate molten liquid, which could result in the benefit of chemical durability. These comments somehow predict the measured shift in chemical compositions met when remelting some of the glasses. Compositions RB6, RB7, and RB6M, which contain Bi_2O_3 instead of UO_2, were made using high atomic weight atom Bi with the idea of avoiding radioactive (however low natural uranium levels) uranium in the development of these glasses. The structural role of Bi can be quite different from that for U ions, mainly reinforcing lateral phosphate chains by high ionic strength $U^{4+,\ 5+,\ 6+}$ ions [27]. It was somehow predicted that the iron phosphate chains having Bi might show lower chemical durability. It was argued that the compositions with Bi needed to be stabilized, and that was the reason for adding MgO to RB6, giving glass RB6M (currently under chemical durability study). Finally, it is noted that compositions RR60, RR62, and RR63 all have important quantities of U oxide and also some additions of Na_2O and Al_2O_3 to regulate the fluidity of the glasses, and with alumina to improve the chemical durability, aiming for better homogenization of the residue (U_3O_8 and possibly Bi_2O_3 and other metal oxides). These latter glasses are currently being studied following the pellet-sintering route of glass powders having the residues.

The DTA curves and dilatometer run for a variety of these glasses (Tables 2 and 3), allowed defining the thermal stability range for them and their tendencies toward crystallization

as it is here the case for both from the surface and/or bulk crystallization [30]. For example, in compositions with U levels, the crystallization even seems clear for compositions with U and large Na contents like RR63; however, for RR60 without Na_2O, and containing around 7 mass/% more Fe_2O_3, a shift toward lower temperatures is also seen in this exothermic peak denoting earlier crystallization for the sodium-rich composition RR63. For the RB6 and RB7 glasses, RB6 contains more bismuth and an equivalent amount of sodium than RB7; however, an exothermic peak is only observed around 998 K, which can be attributed to the greater presence of a modifying oxide such as Bi_2O_3, up to 7.6 mass/% more. On the other hand, the increase in the addition of Bi_2O_3 did not change the fraction of Fe^{2+} ions in these types of iron phosphate glasses as studied in [26]. Although it could even have a reducing effect, which must be demonstrated. Nevertheless, with the incorporation of U, there was a stronger oxidizing effect as indicated by the lower fraction of ferrous ions in the melt.

The results from Fig. 8, compared with the Mössbauer analysis shown in Fig. 9, exhibit that the AR6 sample (with almost three times more uranium than AR4) has a low Fe^{2+} fraction: 0.04. AR4 presents this fraction of Fe^{2+} as 0.35; this increase may be due to AR4 having less uranium in its composition to produce the oxidation of a large amount of iron Fe^{2+} to Fe^{3+} (AR4: 42.2 mass/% Fe_2O_3). The thermogravimetric analysis performed for typical glasses AR1, AR4, AR5, and AR6, all containing UO_2 [18] indicated, together with the Mössbauer measurement of ratios [Fe^{2+}/($Fe^{2+}+Fe^{3+}$)], that Fe^{2+} oxidizes to Fe^{3+} for temperatures in the transformation range (up to T_s, the dilatometric softening point). Apparently, the uranium ion redox reaction strongly changes the Fe^{2+}—Fe^{3+} redox reaction. As noted earlier, the tendency of these glasses to crystallize also appears to be controlled by the Fe^{2+}/($Fe^{2+}+Fe^{3+}$) ratio and possibly by kinetic parameters like the glass viscosity.

The sintering/densification of glassy powder-pellets of iron phosphate compositions containing UO_2 (equivalent to U_3O_8) is shown to be a feasible technique to prepare semisolid (small porosity remaining) blanks containing such oxide residue with high densities, which has a positive impact on the management of radioactive waste, in terms of the reduction in volume occupation for final disposal. Additions of UO_2 to most of the glasses developed at the Centro Atómico Bariloche [16–19, 23–25, 27] increased the glass viscosity, which means the onset in densification occurs at higher temperatures. Likewise, it exhibits higher densification activation energy E_a, from 134 to 188 kJ mol^{-1}, compared to glass without UO_2 (PFeOx) to glass PFeUOx. As proven in the afore-mentioned previous investigations, some of these glasses also showed a low tendency toward crystallization. Furthermore, they exhibited high chemical durability toward water corrosion.

For the case of varying the Na_2O content in the composition of other types of iron phosphate glasses with a high level of UO_2 and specific additions of Na_2O and Al_2O_3, it was found for glass RR63 with 9.8 mass/% Na_2O that initially (847–869 K) the densification-activation energy was very low (43 kJ mol^{-1}). The latter, for the next temperature range 873–893 K, increased to 278 kJ mol^{-1}. These glasses, RR60, RR62, and RR63, are thought to have a high fluidity to improve the waste glass with UO_2 homogenization. Still, composition RR63 also exhibited a clear crystallization exotherm at a rather low 893 K (Fig. 3), and therefore, some specific addition should act on this glass to delay crystallization. As noted in "Thermal behavior of new glasses" section, certain compositions like RR62 appear quite suitable to make waste forms with high content of UO_2 nuclear residue.

Finally, and as discussed in "Differential thermal analysis (DTA) and differential scanning calorimetry (DSC)" section additions of Bi_2O_3 residue as RB iron phosphate glasses decrease the T_g of the glasses, somehow causing a weakening effect of the glass structure. This is the opposite compared to the addition of UO_2 waste to iron phosphate glasses, whereby a stronger glass structure (lower thermal expansion and higher T_S) is induced. The problem of stabilizing the thermal properties (and improving the chemical durability) of RB glasses, for example, through MgO additions, has been analyzed. The enhancement of homogenization of UO_2 within the iron phosphate glass structure by additions of Na_2O, Al_2O_3 in RR6xx glasses or the understanding of chemical durability behavior in PFeUOx or ARx glasses have been successfully addressed during the last twenty years investigation. It appears feasible that the sintering technique can be adopted to make nuclear waste forms rich in UO_2 or Bi_2O_3 or related waste oxides, where techniques like making glass-frits may be used to prepare the powder suitable for waste forms by sintering or axial-hot pressing or through HIP processing.

Conclusions

Vitreous compositions that melt at relatively low temperatures (around 1373 K) with a large amount of uranium oxide (~ 19 mass/%) were achieved. Furthermore, melted phosphate glasses showed low viscosity, higher fluidity, probably related to the addition of Na_2O, which leads to an efficient mixing and decreases the waiting time for chemical homogenization. For bismuth ones, iron phosphate glasses melt around 873–893 K.

The glass compositions designed in this research are thermally stable. However, though some give rise to crystallization (after specific treatment) of some phosphate and pyrophosphate phases, as was detected by thermal analysis methods (DTA/TGA), thermal expansion, and X-ray

diffraction measurements. In composition RR7 containing approximately 14 mass/% UO_2, the activation energy for crystallization was determined, and a value of 184 kJ mol^{-1} was obtained applying the Kissinger method. Another way to estimate the activation energy from DDTA curves applied well.

It was possible to elucidate that the addition of uranium improves the vitreous stability and thus the resistance to crystallization, resulting in stronger glasses with lower thermal expansion coefficients and better properties against water corrosion. Regarding Bi additions, it is inferred that it does not significantly increase the vitreous stability or the properties of chemical durability; however, it seems to favor crystallization at lower temperatures. On the other hand, additions of MgO seem suitable to improve the thermal glass stability.

Sintering these phosphate glasses is possible, giving rise to solid, dense, stable pellets, giving a desirable densification behavior for the waste form sought, which means lower volumes of the final disposal and strong/stable bodies.

Acknowledgements Special thanks are due to the Bariloche Atomic Center groups: Nuclear Materials Department staff, for providing facilities to use their furnaces and raw materials, and Characterization of Materials Department for the SEM, DTA, TEM (Metals Physics Division). Also, to Drs. Sebastián Barolin and Oscar de Sanctis from Universidad Nacional de Rosario Argentina (UNR) for the TGA measurements. Likewise, to Dr. Mónica Aineto from Castilla-La Mancha University (Spain) for the DSC analysis. Equally, to Dr. Flavio Soldera and the Functional Materials Group at Saarland University (Germany) for FIB TEM work, and Dr. Cinthia Ramos at Centro Atómico Constituyentes, and CONICET for Mössbauer analysis. Conicet is thanked for doctoral scholarship and project financial support. The Universidad Nacional de Cuyo and the Joint European Master Program on Advanced Materials Science and Engineering (FPT IRSES Proy Nr 247524 ´NanoCom Network´) are acknowledged for project and travel budgets assignments. Finally, are also recognized the revisions made by the Department of Quality of publications of the Servicio Geológico Colombiano, as well as by Paul Nostrom from UMH-Elche, Spain.

References

1. Hidalgo M, Ma J. Rincón, Fundamentos de la inmovilización de residuos radiactivos en matrices vítreas y vitrocerámicas. Boletín de la Sociedad Española de Cerámica yVidrio. 1987;26:227–34.
2. Rincón JM. Glasses and Glass-ceramics for Nuclear Waste Management, 2nd edition SECV and CIEMAT, Madrid, 1992 and 1st edition ICV-CSIC, Madrid, p. 212. 1987.
3. Ojovan MI, Lee WE. New Development in Glassy Nuclear Wasteforms, Ed. Nova Science Publishers: New York, 2007. p. 126.
4. Day DE. An alternative host matrix base on iron phosphate glasses for the vitrification of specialized waste forms. Environ Manag Sci Progr. 2000. https://doi.org/10.2172/837407.
5. Ciecinska M, Stoch P. The effect of mechanical activation on the thermal reactions of P_2O_5–Al_2O_3–Fe_2O_3–Na_2O phosphate glasses. J Therm Anal Calorim. 2012;108(2):711–5.
6. Ciecinska M, Stoch P, Stoch A, Nocun M. Thermal properties of $60P_2O_5$–$20Fe_2O_3$–$20Al_2O_3$ glass for salt waste immobilization. J Therm Anal Calorim. 2015;121:1225–32.
7. Kuczek J, Jelen P, Sułowska J, Szumera M. Correlation between glass transition effect and structural changes in multicomponent iron phosphate-silicate glasses. J Therm Anal Calorim. 2019;138:4145–53.
8. Kuczek J, Sułowska J, Lach R, Szumera M. The glass formation and crystallization studies on iron phosphate–silicate glasses. J Therm Anal Calorim. 2019;138:1953–64.
9. Goj P, Ciecinska M, Szumera M, Stoch P. Thermal properties of Na_2O–P_2O_5–Fe_2O_3 polyphosphate glasses. J Therm Anal Calorim. 2020;142:203–9.
10. Harrison MT. Current challenges in the vitrification of nuclear wastes in the UK, in Vitrification and Geopolymerization of wastes for immobilization or recycling, In: Jordan MM, Pinet O, Rincón JM Editors, Editorial: UMH and ICG (TC05), Elche, Alicante, Spain, 2019. pp. 45–89.
11. Karabulut M, Marasinghe GK, Ray CS, Day DE, Ozturk O, Waddill GD. X-Ray Photoelectron and Mössbauer spectroscopy studies of iron phosphate glasses containing U, Cs and Bi. J Non- Cryst Solids. 1999;249:106–16.
12. Fernández-Navarro JM, El Vidrio, Ed. CSIC, Madrid, España, 2003. pp. 142–146.
13. Sestak J. The theory and practice of differential thermal analysis, Chapter 12 in: Thermophysical Properties of Solids, In: Sestak J editor, Academia Prague, Elsevier: Amsterdan, 1984. pp. 303–343.
14. Varschavsky A, Sestak J. Applications of differential scanning calorimetry for the study of transformation processes in quenched alloys,Chapter 5 in: Chararacterization Techniques of Glasses and Ceramics. In: Rincón JM, Romero M editors, Springer- Verlag, Berlin, 1999 pp. 85–111.
15. Zarzycki J. In: Scott WD, Massart C Editors, Glasses and the vitreous state, Cambridge University Press: UK, 1991. p. 30; pp. 358–360.
16. Rincón JM, Ramos C, Arboleda P, Oliver CJRG. Vitrification of U_3O_8 in iron aluminium phosphate matrices including Bi_2O_3 as uranium surrogate. Mater Lett. 2018;227:82–5.
17. González-Oliver CJR, Russo DO, Lovey FC, Rincón JM. Iron Aluminium Silico-Phosphate Glasses Including U_3O_8, In: Burakov BE, Alloy AS editors, Scientific Basis for Nuclear Waste Management, MRS (Materials Research Society), Symposium Proceedings, Warrendale, USA, vol. 1193, 2009. pp. 329–336.
18. González Oliver CJR, Lovey FC, Caneiro A, Russo DO, Rodríguez DS, Soldera F, Fiscina JE, Rincón JM. Crystallization of iron phosphate glasses containing up to 19mass/% $UO_{2.67}$. J Non-Cryst Solids. 2010;356:2986–93.
19. Rodríguez DS, Arboleda PA, Russo DO, Soldera F, González-Oliver CJR, Rincón JM. Thermal behaviour of iron aluminium phosphate glasses containing $UO_{2.67}$. Glass Technol Eur J Glass Sci Technol A. 2013;54:111–8.
20. Rincon JM. Principles of nucleation and controlled crystallization of glasses. Polymer- Plast Technol Eng. 1992;31(3–4):309–57.
21. Benavidez E. The Application of DTA/DSC to the study of glass-to- glass-ceramics transformation in glasses from inorganic wastes, In: Thermal analysis applied to complex systems: slags, glasses and ceramics, transworld research network 37/661, Trivandum, Kerala, India, 2013. pp. 33–107.
22. Marotta A, Saiello S, Branda F, Buri A. Activation energy for the crystallization of glass from the DDTA curves. J Mater Sci. 1982;17:105–8.
23. Russo DO, Rodríguez D, Sterba M, Rincón JM, González-Oliver C. Efectos del contenido de óxido de uranio en la estructura de vidrios de ferrofosfatos. Jornadas Sam Conamet- AAS. 2001;2001:835–42.
24. Russo DO, Rodríguez D, Grumbaum N, González-Oliver C. Oxidación y cristalización a altas temperaturas en

vidrios ferrofosfatos. Jornadas Sam- Conamet- Simposio Materia. 2003;2003:995–8.
25. González-Oliver C, Rincón JM, Suárez SG. Análisis PIXE/RBS de vidrios del sistema UO_2-Fe_2O_3–P_2O_5 como inmovilizadores de residuos; Jornadas Sam- Conamet 2018, Bariloche, 2018. pp. 1120–1122.
26. Day DE, Ray CS. A review of iron phosphate glasses and recommendations for vitrifying hanford waste. United States. N. P. 2013. p. 70 https://doi.org/10.2172/1130550
27. Russo DO, Rodríguez DS, Rincón JM, Romero M, González-Oliver C. Thermal properties and crystallization of iron phosphate glasses containing up to 25 mass/% additions of Si-, Al- Na- and U-oxides. J Non-Cryst Solids. 2008;354:1541–8.
28. Mackenzie JK, Shuttleworth R. A phenomenological theory of sintering. Proc Phys Soc Lond Sec B. 1949;62:833.
29. Frenkel J. Viscous flow of crystalline bodies under the action of surface tension. J Phys. 1945;9(5):385–91.
30. Sestak J, Holecek M, Malek J. Preface (pp. 2–6), 12 (pp. 8–27), 13 (pp. 118–137) and 17 (pp. 266–284) chapters, In: Some thermodynamic, structural and behavioral aspects of materials accentuating non-crystalline States, OPS Nymburk, Plzen ZCU, Czech Republic, Pilsen, 2009. p. 624.